Eur. Phys. J. D **1**, 243–254 (1998)

THE EUROPEAN PHYSICAL JOURNAL D

3dnd J = 4, 5 autoionizing levels in Ca: laser optogalvanic spectroscopy and theoretical analysis

S. Assimopoulos[1], A. Bolovinos[1], E. Luc-Koenig[3], S. Cohen[2], A. Lyras[1,a], P. Tsekeris[1], and M. Aymar[3]

[1] Atomic and Molecular Physics Laboratory, Physics Department, University of Ioannina, 451 10 Ioannina, Greece
[2] Institute of Accelerating Systems and Applications, P. O. Box 17214, 10024 Athens, Greece
[3] Laboratoire Aimé Cotton, CNRS II, Bâtiment 505, 91405 Orsay Cedex, France

Received: 20 November 1997 / Accepted: 15 January 1998

Abstract. We report the even parity $J = 4, 5$ autoionizing spectra of calcium below the 3d threshold, investigated by two-step laser excitation from the 3d4s metastables through the 3d4p $^3F_{3,4}$, $^1F_3$ intermediate states and subsequent optogalvanic detection. The 3d4s states are populated by electronic collisions in a d.c. glow discharge sustained in a Ca heat-pipe. More than a hundred resonant transitions have been measured with an accuracy of ~ 0.2 cm^{-1} for the narrow ones using standard laser calibration techniques. The high lying levels are assigned to all expected 3dnd $J = 4, 5$ autoionizing series. Moreover, some 3dng $J = 4, 5$ levels are observed. The theoretical interpretation is achieved by a combination of the nearly *ab initio* eigenchannel R-matrix and multichannel quantum-defect (MQDT) methods as well as by an empirical determination of the MQDT parameters in the phase-shifted formulation. Theoretical energy level positions and excitation profiles are compared with the experimental data confirming the identification of the observed structures. Strong mixing between 3dnd $J = 4$ series is found, while the 3dng ones do not couple with the 3dnd series. Further insight into the strong channel mixing in the studied energy range is provided by a comprehensive review of the excitation profiles in the vicinity of the 4p5p $^3D_3$ perturber as obtained from a number of intermediate levels used in the present and in earlier experiments. Systematic electron correlation trends for Ndnd $J = 4$ series of Ca($N = 3$), Sr($N = 4$) and Ba($N = 5$) are discussed.

PACS. 32.80.RM Multiphoton ionization and excitation to highly excited state (e.g. Rydberg states) – 32.30.Jc Visible and ultraviolet spectra – 32.80.Dz Autoionization

1 Introduction

Alkaline earths are very convenient two-electron systems for atomic physics studies, both experimentally and theoretically. An up-to-date extensive review of the work done on them can be found in [1]. Even parity 3dnl, $J = 0 - 3$, autoionizing levels of Ca have been recently investigated by two-step laser excitation from the 3d4s metastables through the 3d4p intermediate levels [2,3]. In the present work we complete our study of the even parity 3dnl autoionizing levels of calcium up to $J = 5$ by exploiting spectra obtained earlier through the 3d4p $^1F_3$ and performing new measurements through the 3d4p $^3F_{3,4}$ intermediates. The autoionizing Ca levels are detected in a d.c. glow discharge by a two-step laser optogalvanic technique [2]. In this discharge the various Ca 3d4s metastable levels are sufficiently populated by electronic collisions. From these metastables the odd parity 3d4p $^3F_{3,4}$, $^1F_3$ levels are excited in the first excitation step and different 3dnd and 3dng $J = 4, 5$ autoionizing levels are populated in the second step. The simplicity of this experimental method is particularly suited for such high-J levels, which would otherwise require a higher number of laser photons to be reached in a multi-step or a multi-photon excitation scheme from the ground state. The theoretical nearly *ab initio* treatment of the studied levels is by now well developed and comprises a combination of the eigenchannel R-matrix and multichannel quantum-defect (MQDT) methods [1]. An additional empirical determination of phase-shifted MQDT parameters has proved to be quite helpful for the correct assignment of the 3dnd $J = 4$ levels. The phase-shifted MQDT parameters were also used for comparing the channel coupling strength in the $J = 4$ spectrum of Ca to the corresponding ones in the Sr and Ba atoms. Finally, the photoionization cross-section in the vicinity of the 4p5p $^3D_3$ perturber, excited from four different intermediate levels, has been comprehensively analyzed both experimentally and theoretically and further insight into the intricate channel interaction in this energy range has been gained.

[a] e-mail: alyras@cc.uoi.gr

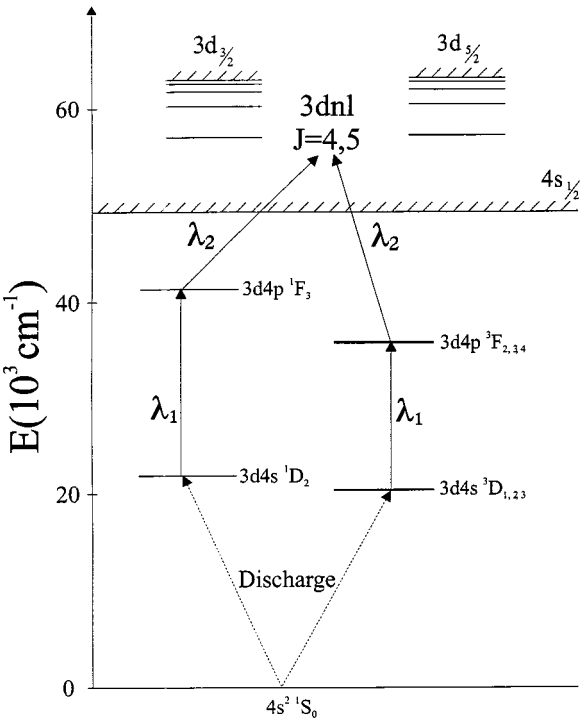

Fig. 1. Ca energy level diagram below the $3d_j$ ionization limits showing the different excitation schemes used in this work.

2 Experimental method and results

The experimental method was introduced by Camus *et al.* [4] and the particular set-up used in this work has been described previously [2,5]. Very briefly, the autoionizing levels under investigation are reached by a two-step laser excitation of Ca atoms in a Ca heat-pipe operating with He as buffer gas at a temperature of ~ 900 ℃. A d.c. glow discharge is maintained at ~ 15 μA across the heat-pipe and Ca excitations produce impedance changes (optogalvanic (OG) effect), which are detected as voltage changes across the ballast resistance of the discharge circuit.

The excitation scheme is shown in Figure 1. The 3d4s metastable levels, at $\sim$ 20 000 cm^{-1} above the ground state, are sufficiently populated by electronic collisions. From these levels, using laser pulses of $\sim 10-20$ μJ and of appropriate wavelength λ_1 from a homemade dye laser oscillator pumped by a fraction of the light from a XeCl excimer laser (Questek 2320), we populate the 3d4p $^3F_{3,4}$, $^1F_3$ levels in the first step. In the second step we excite the 3dnl states using laser pulses of ~ 100 μJ from a second oscillator-amplifier dye laser (Lambda Physik LPD 3000) pumped synchronously by the same XeCl laser. The spectral width of the second dye laser was ~ 0.1 cm^{-1}.

Since the two 3d ionization limits are very close ($\Delta I_{3d} = I_{5/2} - I_{3/2} = 60$ cm^{-1}), the detectability of our method limits us to the region below the $3d_{3/2}$ threshold with $n < 40$. The covered energy range extends from $\sim$ 58 800 cm^{-1} to $\sim$ 62 950 cm^{-1} above the Ca ground state. The identification of the $J = 4, 5$ levels is achieved following the same procedure as in our previous work [2,5]. Specifically, because of the $\Delta J = 0, \pm 1$ selection rules, the observed resonances are due to transitions to $J = 2, 3, 4$ autoionizing levels from the $^1F_3$, $^3F_3$ intermediate levels and to $J = 3, 4, 5$ levels from the $^3F_4$ intermediate. Earlier studies have lead to the identification of the $J = 2, 3$ resonances [2,3]. The remaining resonances are due to $J = 4$ autoionizing levels (observable through all three intermediate levels) and $J = 5$ levels (observable only through the $^3F_4$ intermediate). Figure 2 shows a typical portion of the OG spectrum taken through the 3d4p $^3F_4$ intermediate state. The numbered lines belong to the $3d_{5/2}nd_{5/2}$ $J = 5$ levels with $21 \leq n \leq 40$.

The experimental energies are deduced from the energy positions of the spectral lines, which are quite narrow and symmetric. Absolute energy values are calculated using the known transition energies between bound Ca levels as calibration standards. The accuracy of our results is estimated to be ≈ 0.2 cm^{-1} at low n values ($n \leq 20$) limited essentially by the laser linewidth and signal recording speed. At high n values ($n > 30$), the experimental limit is ~ 0.5 cm^{-1} due to Stark and collision broadening.

In Tables 1, 2 we report the energies and autoionization widths of the experimentally observed 3dnd $J = 4, 5$ autoionizing levels, the relative transition intensities through the $^1F_3$ or $^3F_{3,4}$ intermediates, the corresponding effective quantum numbers relative to the $3d_{3/2}$ and $3d_{5/2}$ ionization thresholds and the theoretical energies and assignments (Sect. 3.1). In a small number of cases the transitions to $J = 4$ levels through some of the intermediate levels are missing for reasons that may depend on low transition probability or coincidence with a stronger line. In such cases the $J = 4$ assignment is secured by resorting to experimental trends of the effective quantum number, intensity and linewidth for the different observed series as well as to the theoretical predictions. We have detected the $n = 6-40$ members of the $3d_{5/2}nd_{5/2}$ $J = 5$ series, the $n = 6-35$ members of the $3d_{3/2}nd_{5/2}$ $J = 4$ series and the $n = 6-27$ members of the $3d_{5/2}nd_{3/2,5/2}$ $J = 4$ series. The quantum defects $\delta_{5/2,4} \cong 0.50 \pm 0.03$ for the $3d_{5/2}nd_{5/2}$ $J = 4$ series and the $\delta_{5/2,5} \cong 0.83 \pm 0.03$ for the $3d_{5/2}nd_{5/2}$ $J = 5$ series are nearly independent of n. On the contrary, the quantum defects for the $3d_{3/2}nd_{5/2}$ and $3d_{5/2}nd_{3/2}$ $J = 4$ series vary widely in the ranges $0.38 \leq \delta_{3/2} \leq 0.85$ and $0.43 \leq \delta_{5/2} \leq 0.82$ respectively.

In Table 3 we report the few 3dng levels we were able to detect through the $^3F_{3,4}$ intermediates, in spite of the weak intensity of the corresponding lines. These levels have very small quantum defects $\delta_{3/2,5/2} \leq 0.02$ and can be ascribed either to the $3d_{3/2}ng_j$ or to the $3d_{5/2}ng_j$ series. However, the near degeneracy of the levels belonging to series converging towards the same $3d_j$ threshold renders impossible the assingnment of either a J or a j value to these levels.

Table 1. Energies relative to the $4s^2$ ground level, linewidths, relative transition intensities via the indicated intermediate levels and effective quantum numbers relative to $3d_{3/2}$ and $3d_{5/2}$ ionization limits for the 3dnd $J = 4^e$ Ca autoionizing levels. The number of significant digits in the effective quantum numbers reflects the accuracy with which the experimental energy was measured. The last two columns give the theoretical energies, calculated from the effective reaction matrix restricted to closed channels, and the assignment of each wavefunction to jj-coupled levels. $d-$ stands for $d_{3/2}$ and d+ for $d_{5/2}$. The numbers in brackets next to the assignments give the percentage weight of the respective jj-coupled components. Peak amplitude estimates: vvs (very very strong), vs (very strong), s (strong), m (medium), w (weak), vw (very weak). The additional symbols have the following meaning: B, overlap with a stronger transition between bound Ca levels; R, overlap with a stronger transition to a neighboring $J \neq 4$ level; NR, not recorded.

E_{exper} (cm^{-1})	Width (cm^{-1})	$^1F_3$	$^3F_3$	$^3F_4$	$\nu_{3/2}$	$\nu_{5/2}$	E_{theor} (cm^{-1})	Assignment
58829.6	1.2	vw	vvs	vvs	5.157	5.119	58834.0	6d-+,d+- [52,48]
59344.1	0.3	s	m	vvs	5.512	5.466	59375.2	6d++ [71]
59463.5	0.3	vs	s	m	5.605	5.557	59488.9	6d+-,d-+ [36,35]
60077.8	0.5	vw	vvs	vvs	6.175	6.110	60080.7	7d-+,d+- [53,47]
60389.7	0.4	w	-	s	6.539	6.463	60408.7	7d++ [64]
60457.2	0.4	s	B	vw	6.627	6.548	60473.4	7d+-,d-+ [32,32]
60836.1	0.4	w	vs	w	7.195	7.094	60838.2	8d-+,d+- [55,45]
61042.9	0.3	w	-	s	7.573	7.456	61055.4	8d++ [52]
61084.7	0.3	s	w	vw	7.657	7.536	61095.6	8d+-,d-+ [26,26]
61331.1	0.3	vw	sh	w	8.218	8.068	61332.9	9d-+,d+- [57,43]
61477.8	0.3	w	vw	-	8.616	8.444	61486.3	9d+-,d-+ [36,27]
61506.5	0.3	s	w	w	8.700	8.524	61514.4	9d++ [63]
61672.0	0.3	w	vvs	m	9.244	9.033	61673.8	10d-+,d+- [59,41]
61781.8	0.3	s	vs	vs	9.667	9.426	61787.6	10d+-,d-+ [46,32]
61804.2	0.3	s	vs	vs	9.760	9.513	61810.2	10d++ [78]
61916.8	0.3	m	vvs	m	10.275	9.988	61918.5	11d-+,d+- [61,39]
62002.9	0.5	s	vs	vs	10.729	10.403	62006.4	11d+-,d-+ [53,35]
62022.7	0.4	s	vs	vs	10.843	10.506	62027.0	11d++ [88]
62098.7	0.3	m	vvs	w	11.313	10.933	62100.0	12d-+,d+- [63,37]
62168.0	0.4	m	vvs	vvs	11.800	11.370	62170.4	12d+-,d-+ [57,37]
62187.0	0.3	m	s	vs	11.945	11.500	62190.4	12d++ [92]
62236.9	0.4	w	vs	B	12.352	11.862	62238.5	13d-+,d+- [64,35]
62295.0	0.3	m	vs	vs	12.883	12.330	62296.5	13d+-,d-+ [58,39]
62313.8	0.2	w	w	vs	13.070	12.494	62316.6	13d++ [96]
62344.8	0.2	m	s	-	13.398	12.778	62346.6	14d-+,d+- [63,36]
62394.5	0.3	vw	vs	vs	13.978	13.279	62395.3	14d+-,d-+ [56,43]
62413.5	0.3	vw	vw	vs	14.221	13.486	62415.9	14d++ [95]
62431.2	0.3	m	w	B	14.458	13.689	62433.0	15d-+,d+- [59,37]
62473.6	0.2	vw	s	w	15.080	14.213	62474.0	15d+-,d-+ [51,49]
62493.3	0.2	vw	vw	s	15.398	14.478	62495.2	15d++ [87]
62502.1	0.5	m	-	-	15.546	14.601	62503.5	16d-+,d+- [49,38]
62561.7	0.3	w	vw	vw	16.680	15.528	62563.1	16d++ [55]
62608.2	0.3	vw	w	B	17.759	16.387	62609.1	17d+-,d-+ [53,40]

Table 1. *Continued.*

E_{exper} (cm^{-1})	Width (cm^{-1})	$^1F_3$	$^3F_3$	$^3F_4$	$\nu_{3/2}$	$\nu_{5/2}$	E_{theor} (cm^{-1})	Assignment
62613.8	0.2	vw	w	m	17.904	16.501	62615.0	17d++ [91]
62630.5	0.3	vw	m	-	18.357	16.854	62631.0	19d-+,d+- [67,32]
62650.2	0.3	vw	m	w	18.939	17.301	62650.6	18d+-,d-+ [55,44]
62658.0	0.2	vw	vw	m	19.185	17.488	62659.1	18d++ [95]
62666.4	0.3	w	w	vw	19.461	17.696	62667.0	20d-+,d+- [62,35]
62684.9	0.4	-	m	vw	20.114	18.182	62685.1	19d+-,d-+ [45,55]
62694.8	0.4	B	w	m	20.491	18.460	62696.0	19d++ [68]
62698.0	0.4	w	-	-	20.618	18.552	62698.7	21d-+,d+- [39,30]
62713.3	0.3	vw	m	vw	21.258	19.014	62713.6	22d-+,d+- [66,34]
62724.6	0.4	B	vw	w	21.770	19.378	62725.2	20d+-,d-+ [51,42]
62728.2	0.4	vw	vw	w	21.941	19.499	62728.9	20d++ [48]
62737.0	0.4	vw	w	-	22.37	19.803	62737.5	23d-+,d+- [69,30]
62749.2	0.4	-	w	w	23.02	20.249	62749.4	21d+-,d-+ [49,51]
62755.2	0.3	-	vw	w	23.36	20.480	62755.9	21d++ [88]
62758.2	0.5	w	-	-	23.54	20.598	62758.7	24d-+,d+- [54,34]
62769.2	0.4	B	w	vw	24.22	21.051	62769.4	25d-+,d+- [67,33]
62776.9	0.4	R	vw	vw	24.74	21.386	62777.4	22d+-,d-+ [48,44]
62779.3	0.4	vw	vw	vw	24.91	21.494	62780.0	22d++ [91]
62785.8	0.4	vw	vw	-	25.38	21.794	62786.2	26d-+,d+- [70,28]
62794.6	0.5	R	vw vw	vw	26.06	22.22	62794.8	23d+-,d-+ [44,56]
62799.4	0.5	-	vw	w	26.46	22.46	62800.0	23d++[72]
62801.2	0.5	w	-	B	26.61	22.55	62801.5	27d-+,d+- [44,29]
62808.8	0.6	vw	vw	-	27.29	22.96	62808.9	28d-+,d+- [72,28]
62815.1	0.5	vw	vw	vw	27.89	23.32	62815.3	24d+-,d-+ [49,49]
62818.0	0.4	vw	vw	vw	28.18	23.49	62818.4	24d++ [94]
62820.8	0.7	vw	R	-	28.47	23.66	62821.1	29d-+,d+- [66,30]
62828.0#	-	R	R	R	29.26	24.10	62827.6	30d-+,d+- [69,31]
62832.3	0.4	vw	vw	vw	29.76	24.38	62832.5	25d+-,d-+ [46,48]
62834.0	0.4	vw	vw	vw	29.97	24.49	62834.3	25d++ [92]
62837.6	0.6	vw	vw	R	30.42	24.74	62837.8	31d-+,d+- [72,26]
62843.0	0.7	R	vw	R	31.14	25.12	62843.2	32d-+,d+- [67,33]
62846.9	0.5	R	vw	vw	31.69	25.41	62847.2	26d+-,d-+ [41,48]
62848.0	0.4	vw	vw	vw	31.85	25.49	62848.4	26d++,d-+ [87,10]
62851.6	0.5	vw	vw	R	32.39	25.77	62851.8	33d-+,d+- [74,25]
62856.3	0.8	-	vw	R	33.15	26.14	62856.4	34d-+,d+- [67,33]
62859.2	0.8	vw	vw	B	33.64	26.38	62859.7	27d+-,d-+ [40,50]
62860.5	0.5	-	vw	vw	33.87	26.49	62860.9	27d++,d-+ [88,10]
62863.3	0.8	vw		R	34.38	26.73	62863.6	35d-+,d+- [75,24]

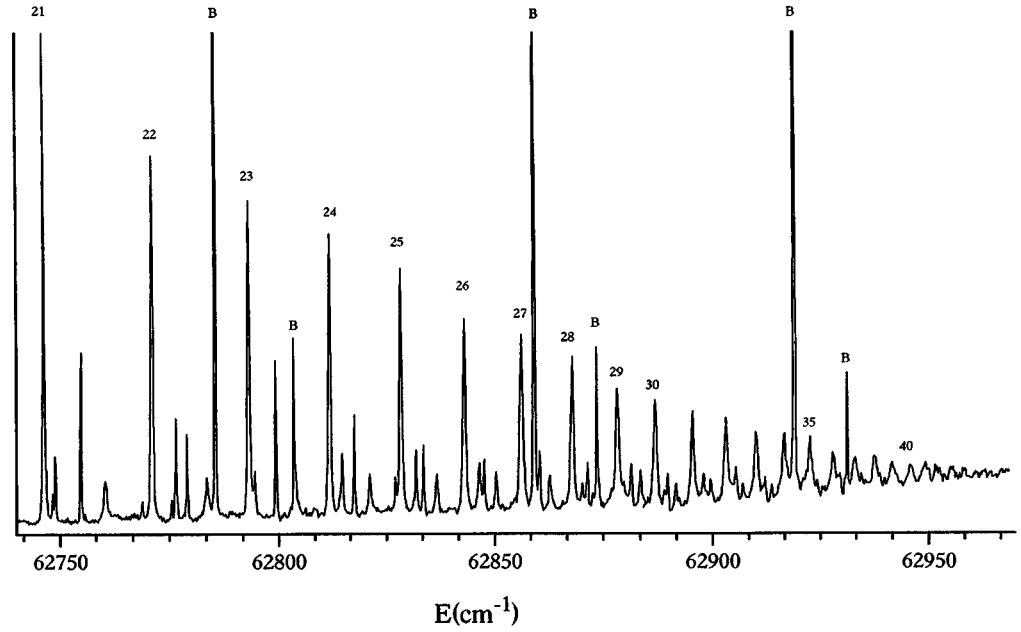

Fig. 2. Typical spectrum in the energy range of 62740 cm^{-1}−62970 cm^{-1} through the 3d4p $^3F_4$ intermediate, showing the $3d_{5/2}nd_{5/2}$ $J = 5$ series for $n = 21$−40. B: transitions between Ca bound levels.

3 Theoretical calculations and analysis of the experimental results

3.1 Energy level positions

3.1.1 Eigenchannel R-matrix/MQDT model

The theoretical analysis for the $J = 4^e, 5^e$ experimental spectra is achieved using a combination of the jj-coupled eigenchannel R-matrix approach and the Multichannel Quantum Defect Theory [1]. This method has been extensively described in earlier studies of the 3dnl $J = 0^e - 3^e$ Rydberg series of calcium [2,3]; only the specific details of the present calculation are given below.

The R-matrix calculation is performed in a reaction volume of $r_0 = 25$ au radius, sufficiently large to describe the 3d4p initial levels in a satisfactory way. As it is shown below the interpretation of the $J = 4^e$ levels involves the strongly coupled $3d_{3/2}nd_{5/2}$ and $3d_{5/2}nd_{3/2}$ channels; a correct description of this mixing requires a precise determination of the $3d_{3/2}$ and $3d_{5/2}$ orbitals and the fine-structure splitting ΔI_{3d} in the Ca^+ ion. The l-dependent model potential, used in earlier papers [2,3] to generate the radial monoelectronic orbitals, was adjusted to reproduce the $Ca^+(nlj)$ energy levels; it resulted though in a too large fine-structure splitting for the 3d ionic level, $\Delta I_{3d} \sim 89$ cm^{-1}. The $l = 2$ orbitals of Ca are very difficult to describe because their fine structure is very sensitive to two effects with opposite contributions. On the one hand, the collapse of the 3d orbital, due to the special position of Ca close to the onset of the 3d transition sequence in the periodic table [6,7], results in a contraction to smaller radii and therefore in an increase of the splitting; on the other hand, the anomalous fine structure effects [8,9] observed in several D and F levels of alkali-like systems and in particular in K, which is isoelectronic to Ca^+, are responsible for anomalously narrow or even inverted fine-structure splittings which cannot be reproduced in a single-electron non-relativistic calculation [10]. In the present work, in order to better describe the $3d_{3/2}$ and $3d_{5/2}$ orbitals the model potential used to calculate them has been optimized to reproduce accurately the experimental Ca^+3d fine-structure splitting. Furthermore, to account for the configuration-dependent collapse of the 3d orbital in excited Ca [7], a larger-than-usual set of two-electron basis wavefunctions has been used including 2371 and 2451 functions for $J = 4^e$ and $J = 5^e$ respectively.

For the calculation of the $J = 4^e$ spectrum, nine interacting channels are employed. Two of them are open, converging to the $4s_{1/2}$ threshold ($4s_{1/2}\epsilon g_{7/2}$, $4s_{1/2}\epsilon g_{9/2}$) and the remaining seven are closed converging towards the $3d_{3/2}$ ($3d_{3/2}nd_{5/2}$, $3d_{3/2}ng_{7/2}$, $3d_{3/2}ng_{9/2}$) and the $3d_{5/2}$($3d_{5/2}\,nd_{3/2}$, $3d_{5/2}\,nd_{5/2}$, $3d_{5/2}\,ng_{7/2}$, $3d_{5/2}\,ng_{9/2}$) thresholds respectively. The calculations for the $J = 5^e$ spectrum include seven interacting channels: two open converging to the $4s_{1/2}$ threshold ($4s_{1/2}\epsilon g_{9/2}$, $4s_{1/2}\epsilon i_{11/2}$) and five closed converging to the $3d_{3/2}$($3d_{3/2}ng_{7/2}$, $3d_{3/2}ng_{9/2}$) and $3d_{5/2}$($3d_{5/2}nd_{5/2}$, $3d_{5/2}ng_{7/2}$, $3d_{5/2}\,ng_{9/2}$) thresholds. The energies of the resonances and the closed-channel admixture coefficients in the wavefunctions are obtained from an effective reaction matrix $K_{\rm eff}$, by reducing the full reaction matrix to the closed channels, after properly eliminating the two open ones [1].

3.1.2 Theoretical results

It is apparent from Table 2 that the agreement between theoretical and experimental energies is very satisfactory for the $3d_{5/2}nd_{5/2}$ $J = 5^e$ levels, the energy differences being less than the autoionization widths except for the lowest lying levels. These levels correspond to pure $3d_{5/2}nd_{5/2}$ jj-coupled levels, the mixing with the 3dng channels being completely negligible.

Table 2. Same as in Table 1 for the $3d_{5/2}nd_{5/2}$ $J = 5^e$ levels (jj-coupling applies).

E_{exper} (cm^{-1})	Width (cm^{-1})	$^3F_4$	$\nu_{3/2}$	$\nu_{5/2}$	E_{theor} (cm^{-1})	Assignment
58860.8	2.4	vvs	5.176	5.138	58865.2	6d++
60109.3	0.9	vvs	6.209	6.143	60112.1	7d++
60868.2	0.6	vvs	7.250	7.146	60870.0	8d++
61364.1	0.5	vvs	8.302	8.148	61365.4	9d++
61705.9	0.3	vvs	9.369	9.149	61706.9	10d++
61951.7	0.2	vvs	10.452	10.150	61952.5	11d++
62134.2	0.2	vs	11.555	11.150	62134.9	12d++
62273.6	0.2	vs	12.680	12.151	62274.1	13d++
62382.3	0.2	vs	13.829	13.151	62382.8	14d++
62468.9	0.2	vs	15.007	14.152	62469.2	15d++
62538.7	0.2	s	16.214	15.150	62539.1	16d++
62596.2	0.2	s	17.461	16.152	62596.4	17d++
62643.9	0.2	s	18.747	17.154	62644.0	18d++
62683.7	0.2	s	20.070	18.150	62684.0	19d++
62717.7	0.2	s	21.453	19.153	62717.8	20d++
62746.6	0.3	m	22.88	20.152	62746.7	21d++
62771.5	0.4	m	24.38	21.149	62771.7	22d++
62793.2	0.5	m	25.95	22.152	62793.3	23d++
62812.1	0.6	m	27.60	23.15	62812.2	24d++
62828.7	0.6	w	29.34	24.15	62828.8	25d++
62843.2	0.7	w	31.17	25.14	62843.4	26d++
62856.3	0.7	w	33.15	26.15	62856.4	27d++
62868.1	0.8	w	35.30	27.16	62868.0	28d++
62878.4	0.8	vw	37.57	28.16	62878.4	29d++
62887.6	0.8	vw	40.0	29.14	62887.8	30d++
62896.2	0.9	vw	42.8	30.16	62896.2	31d++
62903.8	0.9	vw	45.8	31.16	62903.8	32d++
62910.7	0.9	vw	49.1	32.16	62910.7	33d++
62917.2	0.9	vw	53.1	33.19	62917.1	34d++
62922.8	1.0	vw	57.4	34.16	62922.8	35d++
62928.1	NR	vw	62.6	35.17	62928.1	36d++
62933.0	NR	vw	68.9	36.2	62932.9	37d++
62937.5	NR	vw	77	37.2	62937.4	38d++
62941.5	NR	vw	87	38.2	62941.5	39d++
62945.4	NR	vw	101	39.2	62945.3	40d++

For $J = 4^e$ levels, the results are visualized in the expanded Lu-Fano plot (Fig. 3), drawn in the $\nu_{3d_{3/2}}$ (mod. 1) *versus* $\nu_{3d_{5/2}}$ plane. In this plot the full circles correspond to the theoretical energy levels and the open squares to the observed ones. The appearance of a slant branch supporting the levels of the $3d_{3/2}nd_{5/2}$ and $3d_{5/2}nd_{3/2}$ series with large variation in their quantum defects and persisting up to the $3d_{3/2}$ threshold is a signature of the strong $3d_{3/2}nd_{5/2}-3d_{5/2}nd_{3/2}$ channel mixing. On the other hand, this slant branch exhibits narrow avoided crossings with the vertical branch associated with the $3d_{5/2}nd_{5/2}$ levels showing the weakness of the $3d_{3/2}nd_{5/2}$ $-3d_{5/2}nd_{5/2}$ channel mixing. The negligible coupling betwen the 3dnd and 3dng levels and the practically constant calculated quantum defects of the 3dng levels is manisfested by the horizontal and vertical branches which support respectively the $3d_{3/2}ng_j$ and $3d_{5/2}ng_j$ levels and practically cross with the branches supporting the 3dnd

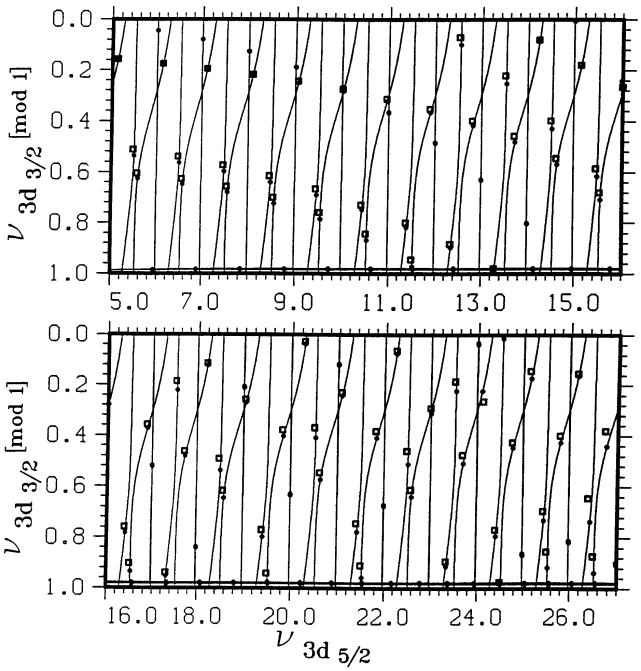

Fig. 3. Expanded Lu-Fano plot of the $J = 4^e$ levels in the $\nu_{3d_{3/2}}$ (mod. 1) *versus* $\nu_{3d_{5/2}}$ plane. The curves and the theoretical energy levels (•) are calculated with the jj-coupled effective reaction matrix $K_{\rm eff}$. Experimental 3dnd energy levels: □.

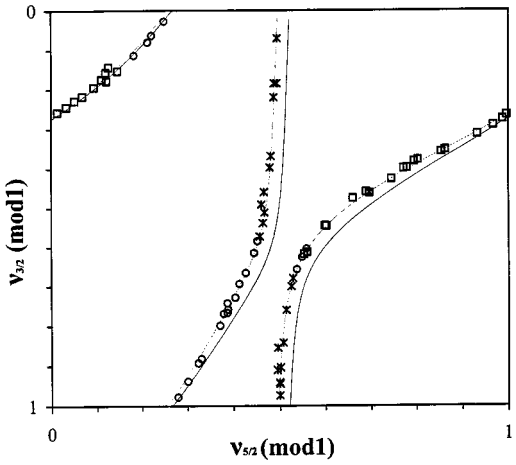

Fig. 4. Reduced Lu-Fano plot of the $J = 4^e$ levels in the $\nu_{3d_{3/2}}$ (mod. 1) *versus* $\nu_{3d_{5/2}}$ (mod. 1) plane. (*): $3d_{5/2}nd_{5/2}$ experimental energy levels. (□): $3d_{3/2}nd_{5/2}$ experimental energy levels. (o): $3d_{5/2}nd_{3/2}$ experimental energy levels. (—): *Ab initio* R-matrix/MQDT result; MQDT parameters calculated at $E = 59400$ cm^{-1} neglecting their energy dependence. (.....): Empirical MQDT fit.

levels. Since the 3dnd and 3dng channels are almost uncoupled, the excitation of the 3dng resonances can be attributed to the mixing of the 3d4p levels with 3dnf or 4png channels; the low strength of this mixing, less than 1%, explains the weak intensity of the corresponding lines. The theoretical energy levels are given in Table 1. One can notice the differences between the calculated and experimental energies for the 3dnd $J = 4$ levels (up to 1% of the ionization energy of the levels). These differences are related to the difficulty for a correct description of the 3dnd channels in Ca [7] as discussed above. The jj-coupled closed-channel admixture coefficients that are calculated to contribute significantly to each particular level are also included in Table 1. Except in the vicinity of energy crossings between levels belonging to $3d_{3/2}nd_{5/2}$ and $3d_{5/2}nd_j$ series, the $3d_{5/2}nd_{5/2}$ levels have a nearly pure jj-character. On the contrary, levels of the $3d_{3/2}nd_{5/2}$ and $3d_{5/2}nd_{3/2}$ series are nearly equally shared between the two channels. Analysis of the wavefunctions of the 3dng $J = 3, 4, 5$ levels reveals that these levels are almost purely jK coupled according to the coupling scheme $|\{3d_j,\ l = 4\}K,\ s,\ J>$. Due to the small exchange electrostatic interaction between the two valence electrons, which have a small overlap in their radial wavefunctions, the energy depends on j and K but not on J (calculated energy difference in the doublet $K = J \pm 1/2$ smaller than 0.05 cm^{-1}). The calculated quantum defects increase slightly, varying in the range of 0.012-0.023, 0.013-0.017 and 0.004-0.008 for the $3d_{3/2}ng$ $K = 7/2$, $9/2$ and $11/2$ series and in the range of 0.012-0.023, 0.014-0.020 and 0.011-0.014 for the $3d_{5/2}ng$ $K = 7/2$, $9/2$ and $11/2$ series, respectively.

3.1.3 Empirical phase-shifted MQDT parameters

The relatively large differences $\Delta E = E_{\rm exp} - E_{\rm theor}$, for the 3d$n$d $J = 4$ levels make their identification difficult, especially for $n > 15$, where the energy spacings of the 3dnd levels with different J values are comparable to ΔE. In order to overcome these difficulties empirical MQDT parameters are determined using the phase-shifted formulation of MQDT [11,12] instead of the eigenchannel formulation [13]. This model includes only the three 3dnd $J = 4$ closed interacting channels: $3d_{3/2}nd_{5/2}$ (channel 1), $3d_{5/2}nd_{3/2}$ (channel 2) and $3d_{5/2}nd_{5/2}$ (channel 3). The 4sεl open channels are ignored, because the resonances are sharp and their widths are much smaller than the spacing between successive series members. The 3dng $J = 4$ channels are also ignored, because of the absence of significant interaction with the 3dnd levels. The phase-shifted MQDT formulation involves two types of parameters: the channel coupling matrix elements of the phase-shifted reaction matrix R'_{ij}, which is real, symmetric, and with zero diagonal elements, and the channel quantum defects $\underline{\mu_i}$ [12]. The phase-shifted reaction matrix is directly related to the reaction matrix obtained in the eigenchannel formulation of MQDT by introducing in the Coulomb functions basis set phase-shifts equal to the quantum defects $\underline{\mu_i}$. For the three 3dnd $J = 4$ interacting channels the maximum number of fitted parameters is six: three quantum defects and three coupling parameters. However, the energy level positions do not depend on the angle β that defines a rotation between the degenerate $3d_{5/2}nd_{3/2}$ and $3d_{5/2}nd_{5/2}$ channels, converging to the same limit [14,15]. Thus the empirical

Table 3. Energies relative to the $4s^2$ ground level, relative transition intensities and linewidths *via* the indicated intermediate state, for the 3dng autoionizing Ca levels. Tentative level assignments appear in the last column, where ng−, ng+ stand for $3d_{3/2}ng$ and $3d_{5/2}ng$ respectively.

E_{exper} (cm^{-1})	$^3F_3$	$^3F_4$	Assignment
5989...	1.7,vw,0.3	1.6,w,0.3	6g-
5995...	1.6,vw,0.3	1.5,w,0.3	}
5995...	3.0,vw,0.3	2.8,w,0.2	6g+
5995...	6.5,vw,0.3	-	
-	-	-	7g-
6076...	6.0,vw,0.5	6.2,vw,0.6	7g+
-	-	-	8g-
6129...	B	4.5,vw,0.3	8g+
-	-	-	9g-
6165...	-	6.3,w,0.3	9g+
6185...	-	4.7,w,0.9	10g-
6191...	5.2,w,0.3	5.0,w,0.5	10g+
6204...	6.0,vw,0.2	6.4,vw,0.4	11g-
6210...	6.9,vw,0.6	6.9,w,0.3	11g+
6219...	1.5,vw,0.6	2.1,vw,0.3	12g-
6225...	2.2,vw,0.3	2.0,w,0.3	12g+
6230...	4.6,vw,sh	4.8,vw,0.5	13g-
6236...	5.3,vw,0.3	5.5,vw,0.3	13g+
6239...	4.5,vs,0.3	4.5,vs,0.3	14g-
6245...	-	5.3,vw,0.3	14g+
6246...	-	7.1,vw,sh	15g-
6252...	-	6.3,vw,0.4	16g-
6252...	-	7.7,vw,0.3	15g+
6257...	-	5.4,vw,0.4	17g-
6258...	6.9,vw,0.4	6.9,vw,0.3	16g+
-	-	-	18g-
6263...	6.2,vw,0.4	5.9,vw,0.3	17g+

Example: 6g- has E_{exp} = 59891.7 cm^{-1} and linewidth $\Delta\nu$ ~0.3 cm^{-1} when seen through $^3F_3$ and E_{exp} = 59891.6 cm^{-1}, $\Delta\nu$ ~0.3 cm^{-1} when seen through $^3F_4$.

fit of the energies, performed by setting $\beta = 0$, reduces the number of empirical parameters to five but does not give any information on the mixing of the $3d_{5/2}nd_j$ channels.

Under these assumptions the MQDT compatibility equation reads as

$$\tan[\pi(\nu_{3/2}+\underline{\mu_1})]\tan[\pi(\nu_{5/2}+\underline{\mu_2})]\tan[\pi(\nu_{5/2}+\underline{\mu_3})] - (R'_{12})^2\tan[\pi(\nu_{5/2}+\underline{\mu_3})] - (R'_{13})^2\tan[\pi(\nu_{5/2}+\underline{\mu_2})] = 0 \quad (1)$$

and the fitting is performed so that (1) as well as the relation between the effective quantum numbers

$$\nu_{3/2} = \nu_{5/2}(1-\nu_{5/2}^2\Delta I_{3d}/\mathrm{Ryd})^{-1/2} \quad (2)$$

are simultaneously satisfied. In the fit only the 3dnd levels with $8 \leq n \leq 19$ are included. Nevertheless, using the empirical parameters, calculated energies agree with the experimental ones to within $\sim$ 2 cm^{-1} for $n = 6, 7$ and to within $\sim$ 0.1 cm^{-1} for $19 \leq n \leq 35$. The values of the empirical parameters extracted from the fit are given in Table 4. The excellent agreement of the empirical fit with experimental data can be seen in the reduced Lu-Fano plot (Fig. 4) drawn in the $\nu_{3d_{3/2}}$ (mod. 1) *versus* $\nu_{3d_{5/2}}$ (mod. 1) plane. Experimental energy levels are identified according to Table 1; $3d_{5/2}nd_{5/2}$ levels appear on the line $\nu_{3d_{5/2}} = 0.5$ (mod. 1), whereas levels belonging to the strongly mixed the $3d_{3/2}nd_{5/2}$ and $3d_{5/2}nd_{3/2}$ are located very close to the curve $\nu_{3d_{3/2}}$ (mod. 1) $= 1.2 - \nu_{3d_{5/2}}$ (mod. 1).

At a given energy, theoretical values for the phase-shifted MQDT parameters, including the β angle, can be directly obtained from the reaction matrix determined in the eigenchannel representation [14]. The *ab initio* R-matrix /MQDT reduced Lu-Fano plot presented in Figure 4 is obtained by neglecting the energy dependence of the theoretical MQDT parameters and using the theoretical values obtained at energy $E \sim 59400$ cm^{-1}. The quality of the nearly *ab initio* R-matrix/MQDT treatment can be appreciated from this curve.

3.1.4 Electronic correlation in the Ndnd J = 4 series of heavy alkaline earths

The spectroscopy of the Ca $J = 4^e$ spectrum completes the existing studies on the $Ndnd$ $J = 4$ series of the most intensively studied alkaline earth atoms Ba ($N = 5$), Sr ($N = 4$), and Ca ($N = 3$). In these series, the coupling among the $Ndnd$, $Ndng$ and $(N+1)pnf$ $J = 4$ channels is almost negligible. The spectrum of Ba has been fitted earlier using the eigenchannel and the phase-shifted MQDT formulations with energy independent

Table 4. Empirical MQDT parameters in the phase-shifted formulation for the Ndnd $J = 4$ series of Ca ($N = 3$), Sr ($N = 4$) and Ba ($N = 5$). The phase-shifted reaction matrix is symmetric. The signs of the coupling parameters cannot be determined from the present fit. The quotation marks in the Channel Label column denote that the assignment for the $3d_{5/2}nd_{3/2,5/2}$ series is only tentative. The data for Ba are taken from Dai *et al.* [16].

Channel No	Channel Label		
1	Nd$_{3/2}n$d$_{5/2}$		
2	"Nd$_{5/2}n$d$_{3/2}$"		
3	"Nd$_{5/2}n$d$_{5/2}$"		
	Ca ($N = 3$)	Sr ($N = 4$)	Ba ($N = 5$)
$\underline{\mu_1}$	0.647	0.641	0.655
$\underline{\mu_2}$	0.662	0.651	0.669
$\underline{\mu_3}$	0.497	0.541	0.590
$\lvert R'_{12}\rvert$	0.716	0.458	0.288
$\lvert R'_{13}\rvert$	0.268	0.245	0.192

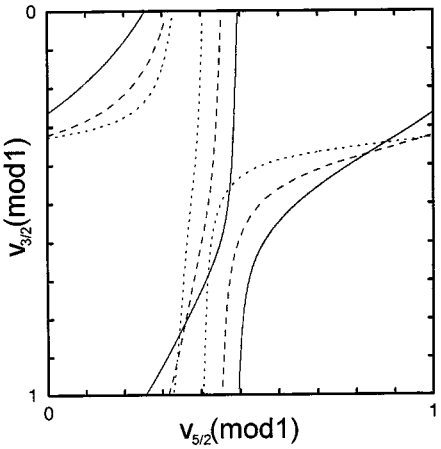

Fig. 5. Reduced Lu-Fano plot of the Ndnd $J = 4$ levels in the $\nu_{3d_{3/2}}$ (mod. 1) *versus* $\nu_{3d_{5/2}}$ (mod. 1) plane for Ca ($N = 3$): (—), Sr ($N = 4$): (- - - - -), Ba ($N = 5$): (.....). The empirical MQDT parameters are obtained in the present study for Ca and Sr, using for Sr the experimental data given in reference [18]. For Ba the empirical parameters given by Dai *et al.* [16] are used.

parameters [16,17]. In order to examine the systematic trends in quantum defects and channel-interaction strengths for all three alkaline earth atoms, we fit the previously published 4dnd $J = 4$ data of Sr [18]. The empirical parameters are assembled in Table 4. Looking at the quantum defects (mod. 1) of each series,we see that $\underline{\mu_1}$ and $\underline{\mu_2}$ are nearly equal and constant for all three atoms, while $\underline{\mu_3}$ increases slowly with increasing atomic number. On the contrary, there is a noticeable change of both coupling parameters (especially $|R'_{12}|$) with their strength increasing with decreasing atomic number. The reduced Lu-Fano plots for Ca, Sr and Ba are superimposed in Figure 5, demonstrating the similarity of the correlation effects in these elements; the decrease in the Nd$_{3/2}n$d$_{5/2}$ − Nd$_{5/2}n$d$_{3/2}$ channel mixing is manifested by the narrowing of the avoided crossing among the corresponding slant branches.

The curves drawn in a Lu-Fano plot and the phase-shifted MQDT parameters are entirely determined by the short-range interactions, essentially the electrostatic interaction between the ionic core and the Rydberg electron, but not by the fine-structure splitting of the Nd$_{3/2,5/2}$ ionic levels, this later quantity imposing only the location of the physical levels on the branches according to equation (2). The Nd$_{3/2}n$d$_{5/2}$ − Nd$_{5/2}n$d$_{3/2}$ $J = 4$ channels in the LS-coupling scheme correspond to the Ndnd ^{1,3}G$_4$ channels and their mixing is typical of the $Nlnl$ ^{1}L$_{J=L}$, ^{3}L$_{J=L}$ channels, as discussed in detail elsewhere [3,19]. In an *ab initio* R-matrix/MQDT calculation, inasmuch as the spin-orbit interaction is negligible within the reaction volume, the LS coupled eigenchannels $Nlnl$ ^{1,3}L$_{J=L}$ can be treated by a two-channel model assuming a decoupling of the Nd$_{5/2}n$d$_{5/2}$ $J = 4$ channel from the other two Nd$_{3/2}n$d$_j$, *i.e.* by imposing $|R'_{13}| = 0$ and $\beta = 0$. The eigenchannels are approximately related to the $Nl_{j-}nl_{j+}$, $Nl_{j+}nl_{j-}(j_\pm = l \pm 1/2)$ dissociation channels by a frame-rotation with angle $\theta = \pi/2$. In the phase- shifted representation these two channels have equal quantum defects and the strength of the mixing of the dissociation channels r_{12}, depends only on $|\Delta\mu_a(L = J)| = |\mu_a(^1L_{J=L}) - \mu_a(^3L_{J=L})|$ the difference between the two eigenchannel quantum defects, where $|\Delta\mu_a| = 0.5$ (mod. 1) corresponds to equally mixed channels. As the energy difference between the $Nlnl$ ^{1}L and ^{3}L Russell-Saunders terms is determined by the exchange electrostatic interaction between the two valence electrons so is $|\Delta\mu_a|$; if one assumes that the Slater integral G^0 prevails in the exchange interaction, then $|\Delta\mu_a(L = J)|$ does not depend on $L = J$ and this explains the similarity in the slant branches supporting the different $Nlnl$ J spectra of a given element with different $J \neq 0$ values. In the present *ab-initio* R-matrix calculation for Ca we have $|\Delta\mu_a| \sim 0.55$ resulting in $|r_{12}| = 0.86$. To estimate these quantities for Sr, we have performed R-matrix calculations for the 4dnd $J = 4^e$ Rydberg series with the l-dependent potential used in the analysis of the $J = 0^e$ and $J = 2^e$ resonances [20]; this results in $|\Delta\mu_a| \sim 0.68$ and $|r_{12}| = 0.54$. For Ba, the phenomenological eigenchannel quantum defects, derived by Aymar *et al.* [17] for the 5dnl $J = 0^e - 5^e$ Rydberg series, confirm the L-independence of $|\Delta\mu_a(L = J)|$ giving $|\Delta\mu_a| \sim 0.22$ and $|r_{12}| = 0.37$. For all three elements, the parameters $|r_{12}|$ deduced by this two-channel model, are of the same order of magnitude as the phase-shifted $|R'_{12}|$ parameters obtained in the complete three-channel treatment. The decrease of the channel coupling between the Nd$_{3/2}n$d$_{5/2}$ and Nd$_{5/2}n$d$_{3/2}$ $J = 4$ series with increasing atomic number is reproduced and attributed to the decrease of $|\Delta\mu_a|$, or, equivalently, of the exchange electrostatic interaction and could be obtained in a phenomenological calculation.

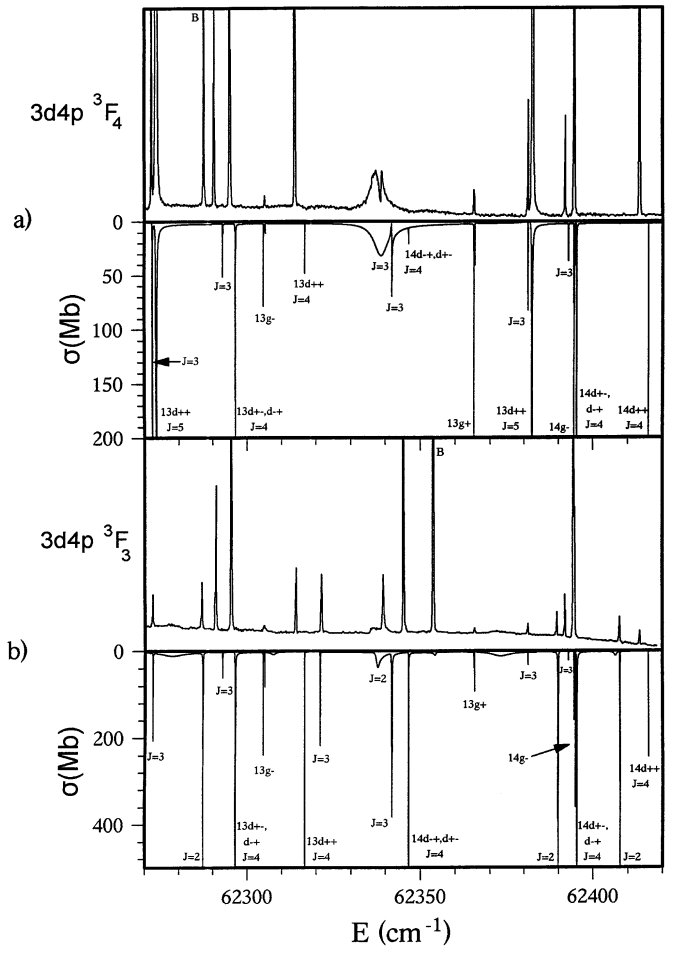

Fig. 6. Experimental (top) and theoretical (below) spectra in the energy range 62270 cm^{-1}−62420 cm^{-1} trough (a) the $^3F_4$ and (b) the $^3F_3$ intermediates. B: transitions between Ca bound levels.

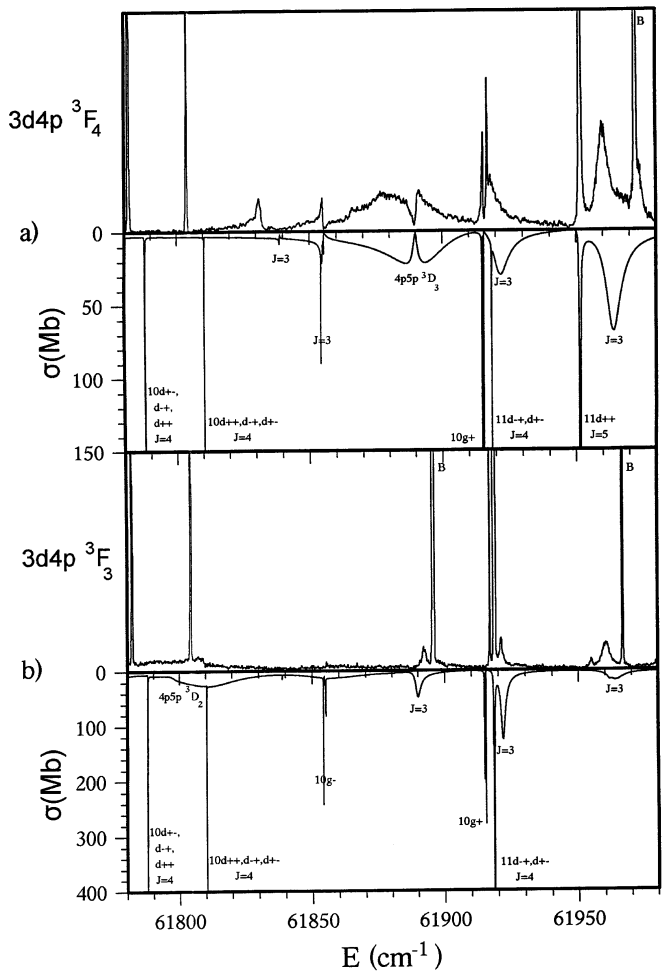

Fig. 7. Experimental (top) and theoretical (below) spectra in the energy range 61780 cm^{-1}−61980 cm^{-1} through (a) the 3d4p $^3F_4$ and (b) the 3d4p $^3F_3$ intermediates. B: transitions between Ca bound levels.

3.2 Photoionization cross section

The calculated photoionization cross sections $\sigma(E)$ for the excitation processes 3d4p $^{1,3}F_{3,4} \rightarrow 3dnl$ $J = 4^e$ with linearly polarized light exhibit resonances, whose energy positions agree with those deduced from the K_{eff} matrix, and whose FWHM give the autoionization widths. For the very narrow resonances (FWHM < 0.1 cm^{-1}) only an upper limit for the autoionization width can be predicted, since the cross-section is calculated in energy steps of 0.15 cm^{-1}. Moreover, only a rough comparison of experimental and theoretical line intensities and shapes is possible since the intensity of the OG signal does not depend solely on the atomic transition cross-section but also on various discharge mechanisms in a complicated way. Furthermore, the theoretical cross sections have not been convoluted to account for the finite resolution (0.2 cm^{-1}) of the experiment. In Figure 6 a part of the OG spectrum, excited through the 3d4p $^3F_3$ and $^3F_4$ intermediates, is shown together with the corresponding R-matrix/MQDT theoretical predictions. The predicted resonances belonging to the $J = 5^e$ levels agree very well with the experimental spectrum both in position and lineshape. The $J = 4^e$ resonances appear as sharp and symmetric lines in the theoretical as well as the experimental spectra, although agreement in the energy level positions is somewhat poorer, as discussed previously.

On the same Figure some $J = 2^e$ or $J = 3^e$ resonances have been identified. The $J = 2^e$ and $J = 3^e$ spectra have been studied in some detail before [3]. In the course of this experiment the spectrum in the vicinity of the previously identified 4p5p $^3D_3$ perturber around 61890 cm^{-1} has also been recorded. These data, shown in Figure 7, complement those already published in reference [3] and offer a comprehensive picture of the excitation of this perturber from a number of different intermediate levels, *i.e.* $^3P_2$, $^1F_3$, $^3F_3$ and $^3F_4$. The recorded lineshapes show either a dip or a peak depending on the intermediate state used in the excitation. Similar behavior was already observed in Ba [21]. In the following we present a theoretical interpretation based on the results of our R-matrix/MQDT

calculations. Although the calculations are performed in jj-coupled basis, the analysis is best understood in LS-coupling. Ten closed, interacting channels are involved, namely 3dns ^{3}D, 3dnd ^{3}D, ^{1}F, ^{3}F and ^{3}G, 3dng ^{3}D, ^{1}F, ^{3}F and ^{3}G and 4pnp ^{3}D, all leading to $J = 3$ levels. Examination of the partial densities of states [1] in each of the above closed channels in the energy range of the perturber shows that those of them associated with the ^{3}D and ^{3}F symmetries exhibit a broad resonance with a width of ~ 20 cm^{-1} including a dip of a much narrower width (~ 2 cm^{-1}) at 61893 cm^{-1}. This broad resonance is identified as the 4p5p ^{3}D corresponding to a strong mixing of ^{3}D channels (70% 4pnp, 19% 3dnd and 11% 3dns). The partial densities of states of the 3dnd channels with ^{1}F and ^{3}G symmetries, present an intense and narrow peak at 61890 cm^{-1} with a width ~ 1.7 cm^{-1}, ascribed to the $3d_{3/2}11d_{3/2}$ level, well described in jj-coupling. Therefore, a first important conclusion is that the different types of resonance structures recorded in the photoexcitation cross section in the vicinity of the perturber are already present in the partial density of states of the various channels. It remains to determine what final-state channels are predominantly excited depending on the 3d4p intermediate level. The relative strength for the excitation of the various closed channels is estimated from *ab initio* values for the dipole matrix elements calculated in the R-matrix/MQDT treatment. Starting from the $^3P_2$ state, only 3dns, 3dnd and 4pnp channels of $^3D_3$ symmetries can be excited. The photoexcitation lineshape is determined by the corresponding partial densities of states and thus a broad structure with a dip is predicted (Fig. 4a in Ref. [3]). Similarly, from the $^1F_3$ intermediate only the 3dnd $^1F_3$ channel can be excited and the cross section is almost proportional to the partial density of states of this channel which is narrowly peaked at the position of the $3d_{3/2}11d_{3/2}$ resonance (Fig. 4b in Ref. [3]). The situation becomes somewhat more complex when the $^3F_3$ and $^3F_4$ intermediates are considered, since then the 3dns, 3dnd and 4pnp channels with $^3D_3$, $^3F_3$ or $^3G_3$ symmetries can be excited. It turns out that from the $^3F_3$ intermediate the dipole matrix elements favor the excitation of ^{3}G symmetry channels and the resulting lineshape is then a narrow peak at the position of the $3d_{3/2}11d_{3/2}$ resonance (see Fig. 7b) following the behavior of the corresponding partial density of states. Analogously, from the $^3F_4$ intermediate the excitation of the $^3D_3$ symmetry dominates and the dip in the photo-excitation lineshape (see Fig. 7a) mirrors the structure of the corresponding density of states.

4 Conclusions

Using a two-step excitation from the 3d4s metastable levels of Ca through the 3d4p $^1F_3$ and $^3F_{3,4}$ intermediates we excited 3dnl $J = 4^e, 5^e$ autoionizing resonances. The analysis was supported by detailed nearly *ab initio* R-matrix/MQDT calculations for the energy positions and photo-excitation spectra. In light of the difficulties to describe correctly the 3d orbital in Ca, because of configuration-dependent orbital collapse and anomalous fine-structure effects, the agreement between theory and experiment is very satisfactory. The 3dnd $^{1,3}G_4$ LS-coupled channels or equivalently the $3d_{3/2}nd_{5/2}$ and $3d_{5/2}nd_{3/2}$ $J = 4$ jj-coupled channels are found to be nearly equally mixed, and this strong coupling is attributed to the strength of the exchange electrostatic interaction between the two valence electrons. Similarities with the 4dnd $J = 4$ levels of Sr and 5dnd $J = 4$ levels of Ba are analysed using empirical MQDT parameters obtained in the phase-shifted formulation; this study reveals the decrease of the strength of the exchange electrostatic interaction with increasing atomic number. The dependence of the excitation profiles in the vicinity of the 3d4p $^3D_3$ perturber on the choice of the intermediate levels used in the excitation process is explained by invoking the nature of the preferentially populated final-state channels.

Numerical calculations were carried out on the Cray 98 belonging to the "Institut de Développement des Ressources en Informatique Scientifique" of the French Centre National de la Recherche Scientifique and on the Cray YMPEL belonging to the "Centre de Ressources en Informatique" of the Université Paris-Sud. The laboratoire Aimé Cotton is associated with the Université Paris-Sud.

References

1. M. Aymar, C.H. Greene, E. Luc-Koenig, Rev. Mod. Phys. **68**, 1015 (1996).
2. S. Assimopoulos, A. Bolovinos, A. Jimoyiannis, P. Tsekeris, E. Luc-Koenig, M. Aymar, J. Phys. B: At. Mol. Opt. Phys. **27**, 2471 (1994).
3. E. Luc-Koenig, A. Bolovinos, M. Aymar, S. Assimopoulos, A. Jimoyiannis, P. Tsekeris, Z. Phys. D **32**, 49 (1994).
4. P. Camus, M. Dieulin, A.E. El Himdy, Phys. Rev. A **26**, 379 (1982).
5. A. Jimoyiannis, A. Bolovinos, P. Tsekeris, Z. Phys. D **22**, 557 (1992).
6. M.A. Khan, J.-P. Connerade, M. Rafique, J. Phys. B: At. Mol. Opt. Phys. **27**, L563 (1994).
7. C. Laughlin, J.E. Hansen, J. Phys. B: At. Mol. Opt. Phys. **29**, L441 (1996).
8. R.M. Sternheimer, Phys. Rev. A **19**, 474 (1979).
9. H.M. Foley, and R.M. Sternheimer, Phys. Lett. **55A**, 276 (1975).
10. E. Luc-Koenig, Phys. Rev. A **13**, 2114 (1976).
11. A. Guisti-Suzor, U. Fano, J. Phys. B **17**, 215 (1984).
12. W.E. Cooke, C.L. Cromer, Phys. Rev. A **32**, 2725 (1985).
13. U. Fano, Phys. Rev. A **2**, 353 (1970); C.M. Lee, K.T. Lu, Phys. Rev. A **8**, 1241 (1973).
14. J.M. Lecomte, J. Phys. B: At. Mol. Opt. Phys. **20**, 3645 (1987).
15. K. Ueda, Phys. Rev. A **35**, 2484 (1987).
16. C.J. Dai, S.M. Jaffe, T.F. Gallagher, J. Opt. Soc. Am. B **6**, 1486 (1989).

17. The same data as in reference [16] have been presented and fitted also by E.A.J.M. Bente, W. Hogervost, Z. Phys. D **14**, 119 (1989) and by M. Aymar, P. Camus and A. El Himdy, Physica Scripta **27**, 183 (1983), but with energy-dependent parameters, so a direct comparison with the present MQDT model is not straightforward.
18. A. Jimoyiannis, A. Bolovinos, P. Tsekeris, P. Camus, Z. Phys. D **25**, 135 (1993).
19. E. Luc-Koenig, M. Aymar, J. Phys. II France **2**, 865 (1992).
20. E. Luc-Koenig, M. Aymar, J.-M. Lecomte, A. Lyras, J. Phys. B: At. Mol. Opt. Phys. (submitted for publication).
21. E. Luc-Koenig, M. Aymar, J. Phys. B: At. Mol. Opt. Phys. **24**, 4323 (1991).